Inorganic Chemistry

Article

pubs.acs.org/IC

Formation of Higher Silanes in Low-Temperature Silane (SiH_4) Ices

György Tarczay,*[,†] Marko Förstel,[‡] Pavlo Maksyutenko, and Ralf I. Kaiser*

Department of Chemistry and W. M. Keck Research Laboratory in Astrochemistry, University of Hawaii at Manoa, Honolulu, Hawaii 96822, United States

Supporting Information

ABSTRACT: A novel approach for the synthesis and identification of higher silanes (Si_nH_{2n+2}, where $n \leq 19$) is presented. Thin films of (d_4-)silane deposited onto a cold surface were exposed under ultra-high-vacuum conditions to energetic electrons and sampled on line and in situ via infrared and ultraviolet−visible spectroscopy. Gas phase products released by fractional sublimation in the warm-up phase after the irradiation were probed via a reflectron time-of-flight mass spectrometer coupled with a tunable vacuum ultraviolet photon ionization source. The formation mechanisms of (higher) silanes were investigated by irradiating codeposited 1:1 silane (SiH_4)/d_4-silane (SiD_4) ices, suggesting that both radical−radical recombination and radical insertion pathways contribute to the formation of disilane along with higher silanes up to nonadecasilane ($Si_{19}H_{40}$).

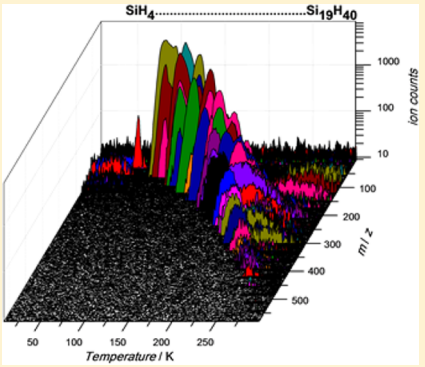

INTRODUCTION

Monosilane (SiH_4) is exploited in significant quantities for the production of amorphous silicon (α-Si:H) by sputtering and chemical vapor deposition (CVD) in semiconductor and solar cell industries.[1] In contrast, higher silanes (Si_nH_{2n+2}) have not been employed in this manner because of their complex synthetic routes and their lack of availability on an industrial scale. However, from an economical viewpoint, they may be preferential starting materials considering the higher efficiency of α-Si:H deposition coupled with lower energy consumption. Furthermore, silanes with more than 10 silicon atoms would represent preferred starting materials because their boiling points are above the temperature of the silicon deposition.[2−4] Besides their importance in the semiconductor technology, higher silanes are considered as hydrogen storage materials, and fuel with monosilane was successfully utilized as an ignition aid in hypersonic NASA X-43A scramjet flights. From the computational chemistry viewpoint, higher liquid silanes were predicted to be usable as full-scale rocket fuels or fuel additives for liquid hydrocarbon-fueled scramjets.[5] Monosilane (SiH_4) is also potentially relevant in astrochemistry and astrobiology.[6,7] As they are co-condensed on interstellar icy grains, the exposure of these astrophysical ices by ionizing radiation in cold molecular clouds likely results in the formation of silicon-bearing molecules. Popularized in the *Star Trek* episode The Devil in the Dark, speculation about silicon chain-based life started in the mid-20th Century; these ideas were compiled in a hypothesis paper of Bains.[8]

Because of their potential role as reagents in the semiconductor industry, novel formation and processing methods for higher silanes have been developed and patented in recent years.[3,5,9,10] The classical, nearly half-a-century-old method of synthesizing higher silanes is based on aqueous acidic hydrolysis of magnesium silicide (Mg_2Si). Fehér and coworkers synthesized and characterized higher silanes up to $Si_{15}H_{32}$.[11−14] Recently, more sophisticated acidic hydrolysis methods were developed such as utilizing organic solvents or fluorosilicic acid (H_2SiF_6), but these methods resulted in only very low yields of a few percent.[3,15,16] Higher silanes can also be prepared by coupling reaction of monosilane (SiH_4) with the help of transition metal catalysts.[3,17] Further, the pyrolysis or photolysis of monosilane (SiH_4) or disilane (Si_2H_6) leads to the formation of longer silane chains, but mostly, or solely, unsaturated subhydrides and amorphous silicon are the main products.[3,18] Since the early 1960s, electrical discharge reactors were patented for the formation of higher silanes. In these reactors, mainly monosilane (SiH_4) or mixtures with argon, neon, hydrogen, and nitrogen were used; these processes also resulted mainly in unsaturated silanes.[3,9] The newest methods suggest that tetrachlorosilane ($SiCl_4$) and molecular hydrogen can be converted in a plasma process to higher-order perhalogenated silanes, which can then be transformed to saturated higher silanes by a treatment with lithium aluminum hydride ($LiAlH_4$).[19] In summary, although multiple processes have been developed to synthesize higher-order silanes, these are not suitable for a large-scale synthesis and/or easy laboratory applications, mainly because these processes do not result solely in the synthesis of saturated higher silanes.[3,9] This fact calls for the elucidation of alternative formation routes of higher silanes. A thorough understanding of the physical and chemical properties of these compounds is crucial for such an undertaking. Earlier infrared spectroscopic studies of electron-irradiated monosilane (SiH_4) ices revealed that various silanes

Received: June 3, 2016
Published: August 11, 2016

DOI: 10.1021/acs.inorgchem.6b01327
Inorg. Chem. 2016, 55, 8776−8785

and their radicals, e.g., SiH_3, Si_2H_6, Si_2H_5, H_3SiSiH, H_2SiSiH_2, and H_2SiSiH, can be formed at 10 K.[7,20] Hiraoka et al. also identified disilane (Si_2H_6) in hydrogen atom-irradiated monosilane (SiH_4) ices at 10 K.[21,22] In addition, the desorption products were investigated by electron impact (EI) ionization coupled with a quadruple mass spectrometer (QMS). Although, because of fragmentation, these studies could not reveal silicon-bearing molecules with mass-to-charge ratios (m/z) beyond m/z 90, on the basis of the temperature-programmed desorption (TPD) curves of the fragment ions, the authors concluded that trisilane (Si_3H_8), tetrasilane (Si_4H_{10}), and a small amount of pentasilane (Si_5H_{12}) sublime.

Here, to better characterize the products formed upon electron exposure of monosilane ices, we couple the TPD approach with tunable vacuum ultraviolet (VUV) photoionization (PI) of the subliming silanes followed by analysis of the ions in a reflectron time-of-flight mass spectrometer (ReTOF-MS). This methodology has been exploited previously to minimize fragmentation of the parent ions;[23,24] therefore, it can aid the identification of higher silanes, which have a kinetically unstable Si−Si bond. Furthermore, the solid-state reaction mechanisms were explored by exploiting a mixture of silane and d_4-silane. The results of this study are important both for the development of nontraditional production routes of higher silanes and for understanding the mechanistical processes taking place in silane-containing astrophysical ices.

EXPERIMENTAL SECTION

The experiments were performed in a contamination-free ultra-high-vacuum stainless steel chamber evacuated to an ultrahigh vacuum of a few 10^{-11} Torr, exploiting magnetically suspended turbomolecular pumps coupled with oil-free scroll backing pumps.[25,26] Briefly, a rhodium-coated silver wafer is mounted onto a rotatable coldfinger made of oxygen-free high-conductivity copper (OFHC) cooled to 5.5 K by a closed-cycle helium refrigerator (Sumitomo Heavy Industries, RDK-415E). The substrate can be freely rotated within the horizontal plane via a differential pumped rotational feedthrough (Thermoionics Vacuum Products, RNN-600/FA/MCO) and also translated in the vertical axis through a UHV compatible bellows (McAllister, BLT106). Gas phase silane (SiH_4, Linde, 99.999%) or d_4-silane (SiD_4, Linde, ≥99% D) was condensed onto the substrate by introducing the gas into the main chamber through a glass capillary array at a pressure of 2.5×10^{-8} Torr. The ice thickness was determined in situ via laser interferometry with a HeNe laser (CVI Melles-Griot, 25-LHP-230) operating at 632.8 nm.[27,28] With a refractive index of 1.4 ± 0.2, a thickness of 680 ± 100 nm was derived. This value is consistent with the optical thickness fitted for the interference pattern observed in the ultraviolet−visible (UV−vis) spectra (UV−Vis Spectroscopy and Figure 3). The ices were then isothermally irradiated for 8 or 60 min with 5 keV electrons at fluxes of 1×10^{11} electrons s^{-1} cm^{-2} over an area of 1.0 ± 0.1 cm^2 at an angle of incidence of 70° relative to the substrate normal. The averaged penetration depth of the energetic electrons was calculated via Monte Carlo simulations (CASINO)[29] to be 370 ± 50 nm. This penetration depth is smaller than the thickness of the deposited ices to ensure that the energetic electrons interact with only the ices, and not with the substrate. Utilizing densities of 0.77 ± 0.03 g cm^{-3},[30] the doses deposited into the ice sample were determined on average to be 0.5 ± 0.1 and 3.6 ± 0.4 eV per silane molecule in the 8 and 60 min irradiation experiments, respectively. The ices were monitored during the irradiation using a Fourier transform infrared spectrometer (FTIR, Nicolet 6700) in the range from 6000 to 500 cm^{-1} at 4 cm^{-1} resolution in intervals of 2 min and via a Thermo Nicolet Evolution 600 UV−vis spectrometer in the 190−500 nm spectral window using a 1 nm step size, a 2 nm bandwidth, and a 60 nm min^{-1} scan rate.

After the irradiation, the sample is kept isothermal at 5.5 K for 1 h. After this, a temperature-programmed desorption (TPD) experiment was conducted to sublime the ice and any products by warming the irradiated samples to 300 K at rates of 0.5 K min^{-1}. During the sublimation, the molecules were analyzed by a reflectron time-of-flight mass spectrometer (Jordan TOF Products, Inc.) after photoionization (PI-ReTOF-MS) at 118.2 nm (10.49 eV).[25] The pulsed (30 Hz) coherent vacuum ultraviolet (VUV) light was generated via four-wave mixing using xenon (Specialty Gases, 99.999%) as a nonlinear medium. The third harmonic (354.6 nm) of a high-power pulsed neodymium-doped yttrium aluminum garnet laser (Nd:YAG, Spectra Physics, PRO-250, 30 Hz) underwent a frequency-tripling process ($\omega_{uv} = 3\omega_1$) to yield the 118.2 nm photons at levels of ~4×10^{11} VUV photons per pulse.[31] The xenon was pulsed into an evacuated mixing chamber at an operating pressure of ~3×10^{-4} Torr. In separate experiments, 129.15 nm (9.60 eV) photons were generated by resonant four-wave mixing ($\omega_{uv} = 2\omega_1 - \omega_2$) in Krypton ($8 \times 10^{-4}$ Torr). For this purpose, 202.3 nm (6.13 eV, ω_1) light was generated utilizing a dye laser (Sirah, Cobra-Stretch) containing a mixture of Rhodamine 640 and Rhodamine 610 dyes (Exciton), which was pumped by the second harmonic (532 nm, 2.33 eV) of the fundamental of a Nd:YAG laser (1064 nm, 1.17 eV; Spectra Physics, PRO-270-30) and frequency tripling of the dye laser output (606.9 nm, 2.04 eV) using β-BaB_2O_4 (BBO) crystals (44° and 77°). Second, the 466.7 nm (2.66 eV, ω_2) light was produced by using the third harmonic (354.6 nm, 3.49 eV) of the 1064 nm (1.17 eV) fundamental of a Nd:YAG laser (Spectra Physics, PRO-250-30) to pump a dye laser (Sirah, Precision Scan) containing Coumarin 460 dye. The VUV light was separated from the fundamental using a lithium fluoride (LiF) biconvex lens[32] (ISP Optics) based on distinct refractive indices of the lens material for different wavelengths and then directed 1 mm above the ice surface.[31] The photoionized molecules were extracted to the direction of the focusing regions by an extraction plate (−190 V). Mass-to-charge ratios were determined on the basis of the arrival time of the ions at a multichannel plate; the signal was amplified with a fast preamplifier (Ortec 9306, 1 GHz, AC coupled) and recorded using a bin width of 4 ns, which was triggered at 30 Hz (Quantum Composers, 9518).

RESULTS AND DISCUSSION

Infrared Spectroscopy. Pure silane ices exposed to energetic electrons at 10 K were already investigated previously via FTIR spectroscopy.[7] Therefore, only a brief summary is provided here, and we will concentrate on new information not published previously. The infrared spectra of the deposited silane and d_4-silane ices are shown in Figures 1 and 2, respectively. These spectra are dominated by the infrared active ν_3 and ν_4 modes with the infrared inactive ν_2 mode barely recognizable. The lattice mode (α) was also observed via the combination bands with the ν_3 and ν_4 fundamentals. These absorptions range within 3 cm^{-1} compared to the previously reported wavenumbers.[7,20] The main difference between the previously recorded data and the data presented here is the relative intensity of the combination modes of the silane vibrations with the lattice modes holding a considerably lower intensity in the spectra presented here. This reveals that these ices are amorphous to a higher degree, which is a consequence of the lower deposition temperature (5.5 K compared to 10 K) and the lower deposition rate used in the study presented here.

On the basis of the FTIR spectra, the response to the irradiation is dictated by the decomposition of the silane molecules to atomic hydrogen and to the silyl radical (SiH_3). The latter was observed after 2 min via the difference spectrum via the ν_2 band at 722 cm^{-1}.[20] The three remaining fundamentals of the silyl radical are difficult to monitor because they overlap with those fundamentals of the silane molecule. Therefore, they cannot easily be recognized in the unprocessed infrared spectrum, but they are clearly visible in the difference

DOI: 10.1021/acs.inorgchem.6b01327
Inorg. Chem. 2016, 55, 8776−8785

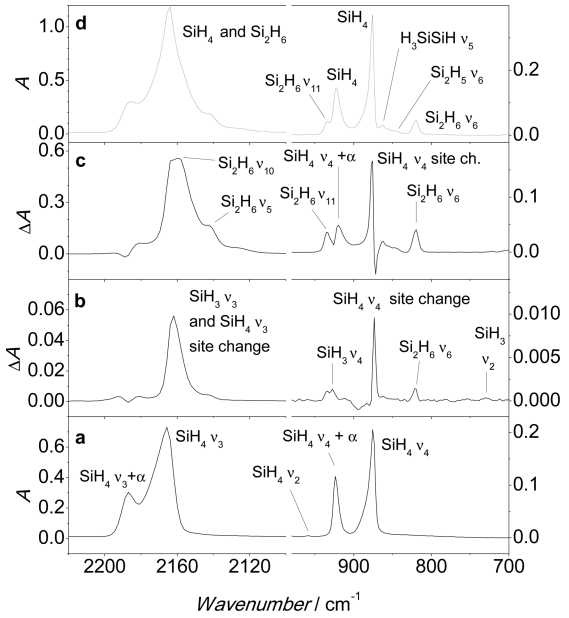

Figure 1. (a) Infrared spectrum of the deposited silane (SiH_4) ice at 5.5 K. (b) Difference spectrum as obtained by subtracting the spectrum recorded before the electron irradiation from that recorded after electron irradiation for 2 min. (c) Difference spectrum as obtained by subtracting the spectrum recorded before the electron irradiation from the one recorded after electron irradiation for 40 min. (d) Infrared spectrum measured after electron irradiation of the silane (SiH_4) ice for 60 min. α is a lattice vibrational mode, and bands appearing in the difference spectra due to band shape change caused by the changing environment of SiH_4 are labeled "site change".

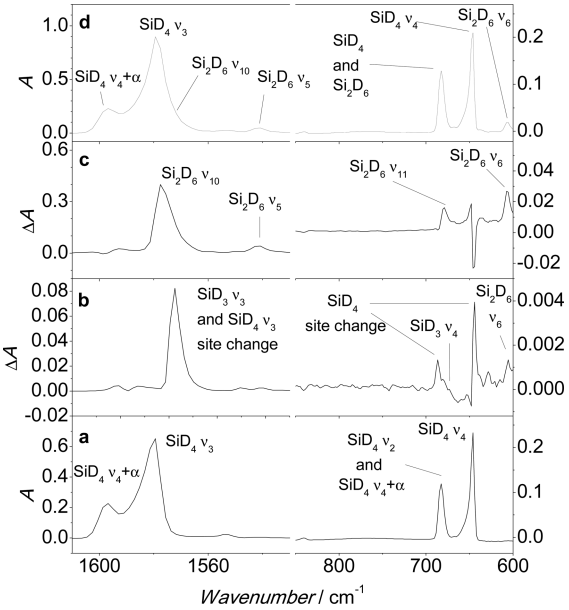

Figure 2. (a) Infrared spectrum of the deposited d_4-silane (SiD_4) at 5.5 K. (b) Difference spectrum as obtained by subtracting the spectrum recorded before the electron irradiation from that recorded after electron irradiation for 2 min. (c) Difference spectrum as obtained by subtracting the spectrum recorded before the electron irradiation from that recorded after electron irradiation for 40 min. (d) Infrared spectrum measured after electron irradiation of the d_4-silane (SiD_4) ice for 60 min. α is a lattice vibrational mode, and bands appearing in the difference spectra due to band shape change caused by the changing environment of SiD_4 are labeled "site change".

spectrum (Figure 1). Here, the band at 927 cm^{-1} can be assigned to ν_4, which was previously observed at 925 cm^{-1} in an argon matrix.[33] The strong band at 2162 cm^{-1} corresponds mostly to the Si−H stretching mode of SiH_4, which appears in the difference spectrum because of the site change around the molecule, and the ν_3 fundamental transition of the silyl radical likely contributes to this peak. This is consistent with (unscaled) B3LYP/6-311G** harmonic frequency computations that predict an intense band for gaseous SiH_3 at 2233 cm^{-1}, a wavenumber ~9 cm^{-1} smaller than that for SiH_4.[20] The ν_1 fundamental of the silyl radical is predicted to be very weak, overlapping with stronger bands of higher-order irradiation products; therefore, it cannot be unambiguously identified. Considering the d_4-silane ice, the formerly identified ν_2 band of d_3-silyl (SiD_3) at 540 cm^{-1} is out of our spectral region, while the band at 669 cm^{-1}, identified as ν_4 of d_3-silyl, appears as a weak feature in the difference spectrum (Figure 2). Because of an overlap with d_4-silane and higher-order products, the weak ν_1 band of the d_3-silyl radical cannot be identified, while the ν_3 transition likely contributes to the band at 1578 cm^{-1}. The bands of another possible reaction intermediate, SiH_2 (observed at 995, 1973/1976, and 1993 cm^{-1} in Ar)[33] and SiD_2 (729/719, 1436, and 1439 cm^{-1} in Ar),[33] cannot be identified in the IR spectra. Because according to B3LYP/6-311G** computations the intensities of the molar absorptions of the most intense bands of SiH_2 and SiH_3 are on the same order of magnitude, either the production of SiH_2 is less effective or its lifetime in the matrix is shorter than that of SiH_3. It should also be noted that even the peaks of SiH_3 are very weak and are quite noticeable only in the difference spectra corresponding to early irradiation times.

The band intensities of the silyl radical reach their maximum intensity in a few minutes, and at longer irradiation times, other intense bands became dominant in the difference spectra. Unlike the intensity of the bands of the silyl radical, the intensities of these bands are continuously increasing during the 1 h irradiation, which reveals that they belong to more stable species. Some of these peaks could be attributed to the disilane molecule (Si_2H_6) depicting intense bands at 2158 (ν_{10}), 2243 (ν_5), 935 (ν_{11}), and 821 (ν_6) cm^{-1}. (In the Ar matrix, intense bands of Si_2H_6 were observed at 2158 and 841−835 cm^{-1}.[33]) For d_6-disilane (Si_2D_6), the corresponding bands are observed at 1577 (ν_{10}), 1542 (ν_5), 679 (ν_{11}), and 606 (ν_6) cm^{-1} (Figure 2). Among the species identified previously in electron-irradiated ices,[7,20] the disilyl radical (Si_2H_5) can also be unambiguously identified at 844 cm^{-1} (ν_6). Additionally, very weak bands of silylsilylene (H_3SiSiH, ν_5) and disilenyl (H_2SiSiH, ν_5) radicals appeared at 867 and 653 cm^{-1}, respectively. Because of the overlap with the nearby strong band of silane, the ν_{11} band of disilene (H_2SiSiH_2) observed previously at 898 cm^{-1} cannot be observed; this band is visible only after sublimation of silane.[20] The bands of the corresponding deuterated species were not observed, because they either overlap with bands of d_4-silane or are outside of our investigated spectral region.

UV−Vis Spectroscopy. The UV−vis spectra recorded before and after electron irradiation of the silane ice for 1 h are displayed in Figure 3. The absorption bands are superimposed by strong interference features in both spectra. Because the thickness and refractive index of the film slightly changed during the irradiation, a simple subtraction of the two spectra cannot be applied to remove the interference bands. To obtain experimental UV−vis spectra free from interference patterns,

DOI: 10.1021/acs.inorgchem.6b01327
Inorg. Chem. 2016, 55, 8776−8785

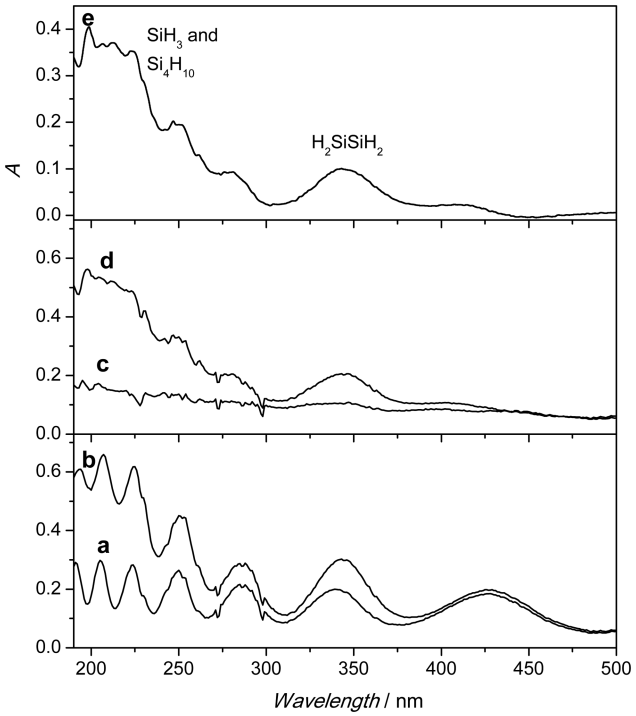

Figure 3. (a) UV−vis spectrum of the deposited silane ice before irradiation. (b) UV−vis spectrum recorded after irradiation for 1 h. (c and d) Absorption spectra of spectra a and b, respectively, after elimination of interference patterns. (e) Difference between spectra c and d. Fitting of eq 1 resulted in a d of 560^{+0}_{-41} nm and an n_2 of $1.3375 + 25/(\lambda - 120)$ (before irradiation) and an n_2' of $1.01n_2$ (after irradiation). The assignments are tentative and are based on and consistent with the assignments of the IR spectra.

the interference was derived theoretically by employing a "two interfaces between three media" model generalized for complex refractive indices $n_i + ik_i$.[34] The first medium is vacuum ($n_1 = 1$); the second is (d_4-)silane ice with unknown dispersion curves, and the third is the rhodium coating, whose complex refractive index components (n_3 and k_3) are known.[35] Within the limit that the relatively weak absorbance of the silane film cannot noticeably change the phase of the interference fringes, we set $k_2 = 0$ to simulate and subsequently subtract the oscillatory parts of the spectra. The real part of the refractive index was sought in the form

$$n_2(\lambda) = A + B/(\lambda - C) \quad (1)$$

with the three fitting parameters A, B, and C. When these parameters and the film thickness value were varied, oscillatory parts of UV−vis spectra of (d_4-)silane ices measured after deposition were fitted. Then a small variation in the refractive index was introduced to account for the small shifts of the interference fringes caused by irradiation. In the next step, the oscillatory components obtained by the model were subtracted from the corresponding experimental spectra. The final result, i.e., the absorbance curve appearing during the irradiation process, is obtained by subtracting the processed spectra to those recorded after and before irradiation [Figure 3, top panel (silane); Supporting Information for d_4-silane; the fitted refractive indices as a function wavelength are also shown in the Supporting Information].

This spectrum depicts a strong absorption band between 190 and 300 nm with a maximum at ∼200 nm. This coincides with the observed $\tilde{A} \leftarrow \tilde{X}$ transition of the silyl radical (SiH_3)[36] and with the absorption of tetrasilane (n-Si_4H_{10}).[37] Lower silanes (e.g., Si_2H_6 and Si_3H_8) have absorption bands only below 200 nm.[38] A weaker absorption is observed with a maximum at ∼345 nm. The carrier of this band is most likely disilene (H_2SiSiH_2); its absorption maximum was observed at 329 nm in an argon matrix.[39]

Mass Spectrometry. To investigate the products that desorb from the surface, the silane and d_4-silane ices were heated at a rate of 0.5 K min^{-1}. Figure 4 shows the PI-ReTOF-MS data obtained by photoionizing the desorbed species by 10.49 eV (and 9.60 eV) photons as a function of temperature from 5.5 to 300 K (or 320 K). Figures 5 and 6 represent the associated TPD profiles of individual ions. In the mass spectra, the progression of silanes ($Si_nH_{2n+2}^+/Si_nD_{2n+2}^+$) dominates (Tables 1 and 2 and Figure 4). The most intense peak belongs to disilane ($Si_2H_6^+/Si_2D_6^+$; $IE_{adiabatic}$ = 9.74 eV[40]) with a maximal ion count in the TPD curves at 94.5 K. Note that silane (SiH_4) cannot be ionized considering its ionization energy (IE) of 11.00 eV ($IE_{adiabatic}$),[41] which is above the 10.49 eV photons exploited here. The largest mass observed in the progression of the subliming molecules of the silane ices is m/z 572 with a maximum in the TPD curve at ∼300 K. This can be identified as $Si_{19}H_{40}^+$, which contains four more silicon atoms than the largest saturated silane observed so far.[3]

Besides the silanes, a dominant progression can be linked to silenes ($Si_nH_{2n}^+/Si_nD_{2n}^+$) from n = 2 to n = 17 and 12 (for silane and d_4-silane, respectively). A closer inspection of the TPD profiles with $n < 6$ reveals that their maxima are at the same temperatures as those of the saturated counterparts ($Si_{n+1}H_{2n+4}^+/Si_{n+1}D_{2n+4}^+$). Moreover, the TPD profiles at low temperatures depict identical patterns (Figures 5 and 6) for the $Si_nH_{2n}^+/Si_nD_{2n}^+$ and the corresponding $Si_{n+1}H_{2n+4}^+/Si_{n+1}D_{2n+4}^+$ species. At the higher-temperature side of the TPD maxima corresponding to the mass of the $Si_{n+1}H_{2n+4}^+$ species, an additional signal can be observed, as well. These ion counts do not belong to $Si_{n+1}H_{2n+4}^+$, but to the heavier isotopomers of $Si_{n+1}H_{2n+2}^+$. This observation suggest that the $Si_nH_{2n}^+/Si_nD_{2n}^+$ species are dominantly or solely formed by SiH_4/SiD_4 elimination after ionization from the $Si_{n+1}H_{2n+4}^+/Si_{n+1}D_{2n+4}^+$ ion, but not by the ionization of the neutral Si_nH_{2n}/Si_nD_{2n} molecules. This explanation is in line with the experimental and computational results of Dopfer et al.[42] Dopfer et al. suggested that the relative energy of silane (SiH_4) with disilene cation ($H_2Si = SiH_2^+$) is only 0.7−1.0 eV higher than that of $Si_3H_8^+$. Furthermore, these authors identified a hydrogen-bridged structure, $H_3Si{-}H{-}SiH_2{-}SiH_2^+$, with an energy that is only ∼0.1 eV higher than that of the classical $H_3Si{-}SiH_2{-}SiH_3^+$ species; both isomers are connected by a barrier of 0.8 eV. Because the energy of the ionizing photon is more than 1 eV higher than the typical adiabatic ionization energies (∼8.8 to ∼9.2 eV) of higher silanes,[43] it is very likely that the classical $Si_{n+1}H_{2n+4}^+/Si_{n+1}D_{2n+4}^+$ ions isomerize to the hydrogen-bridged isomers, which can fragment then via silane and d_4-silane elimination to $Si_nH_{2n}^+/Si_nD_{2n}^+$.

The $Si_{n+1}H_{2n+4}^+/Si_{n+1}D_{2n+4}^+$ species, which decompose via silane/d_4-silane elimination before they reach the reflectron region of the time-of-flight instrument, are revealed via the corresponding ions of the different isotopomers of $Si_nH_{2n}^+/Si_nD_{2n}^+$. In the mass spectra (see the Supporting Information), broad, unresolved peaks also appeared, for example, in the mass ranges of m/z 72−78, 95−103, approximately 120−130, 145−157 (the last two coincide with mass-resolved peaks of higher-

DOI: 10.1021/acs.inorgchem.6b01327
Inorg. Chem. 2016, 55, 8776−8785

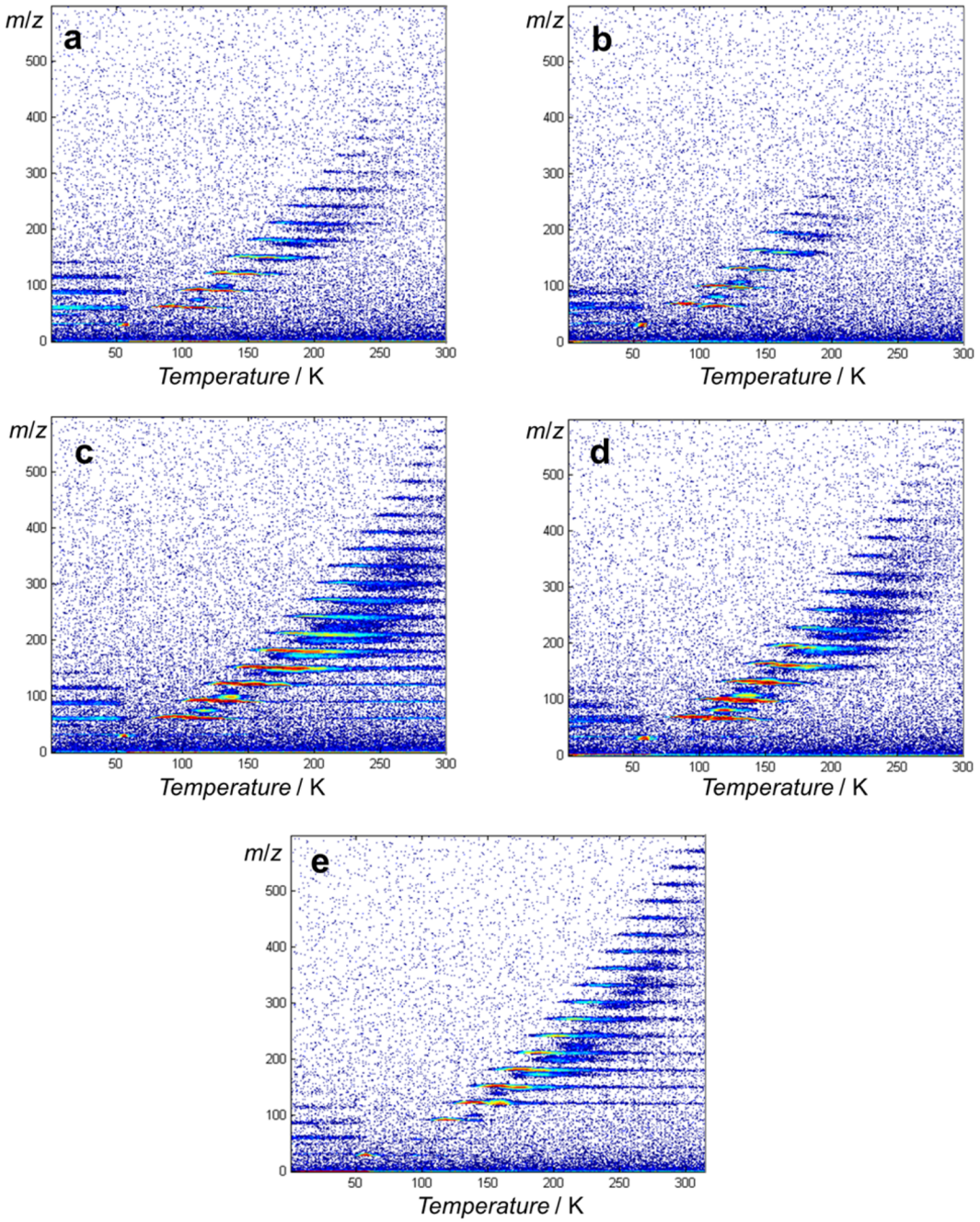

Figure 4. PI-ReTOF-MS data as a function of sublimation temperature as irradiated silane and d_4-silane ices were heated from 5.5 to 300 K: (a) SiH_4, small dose, 10.49 eV photon energy; (b) SiD_4, small dose, 10.49 eV photon energy; (c) SiH_4, large dose, 10.49 eV photon energy; (d) SiD_4, large dose, 10.49 eV photon energy; and (e) SiH_4, large dose, 9.60 eV photon energy.

order silanes), 166−176, 194−205, and 220−235 for irradiated silane ices and 78−86, 104−111, 125−137, 152−170, 175−190 (the last four coincide with mass-resolved peaks of higher-order deuterated silanes), and 204−216 for irradiated d_4-silane ices. These are metastable $Si_{n+1}H_{2n+4}^+/Si_{n+1}D_{2n+4}^+$ species that fragment in or after the reflectron region. Because the intensities of these peaks are similar to the intensities of the parent ions and the corresponding $Si_nH_{2n}^+/Si_nD_{2n}^+$ species, we can conclude that the lifetimes and times of flight of these species are on the same order of magnitude, i.e., in the range of 10−200 μs. For $n < 6$, the TPD profiles of these unresolved mass peaks match very well with the TPD peaks of the corresponding $Si_{n+1}H_{2n+4}^+/Si_{n+1}D_{2n+4}^+$ species.

The data recorded at a photoionization energy of 9.6 eV further support the idea that for a small number of silicon atoms, the $Si_nH_{2n}^+/Si_nD_{2n}^+$ species are solely, or exclusively, generated by fragmentation of $Si_{n+1}H_{2n+4}^+/Si_{n+1}D_{2n+4}^+$ species. At this photon energy, the intensity of the peaks corresponding to $Si_2H_4^+$, $Si_2H_6^+$, and $Si_3H_6^+$ and of the corresponding unresolved peaks is very small; the peak intensity of the $Si_3H_8^+$ isotopomers is lower than the intensity of the peaks of higher-order silanes in the spectrum observed at a 10.49 eV photon energy. In the case of ionization, both $Si_2H_6^+$ and $Si_3H_6^+$ would appear, because the adiabatic ionization energies of Si_2H_6 (9.74 eV) and Si_3H_6 (~9.2 eV) are lower[43] than the photon energy (10.49 eV) in our experiments.

DOI: 10.1021/acs.inorgchem.6b01327
Inorg. Chem. 2016, 55, 8776−8785

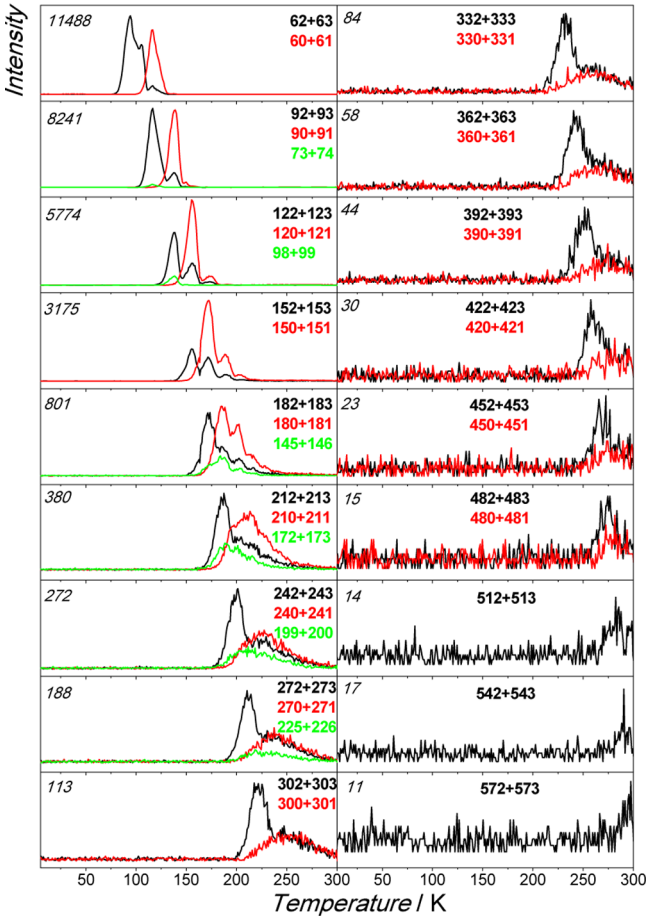

Figure 5. PI-ReTOF-MS data as a function of temperature for the indicated masses (top right in bold with formula) of the large-dose-irradiated silane sample. To obtain a better signal-to-noise ratio, two mass channels were integrated. The strongest peak intensity is shown on the left in italics. The photon energy was 10.49 eV. See the small-dose TPD curves in the Supporting Information.

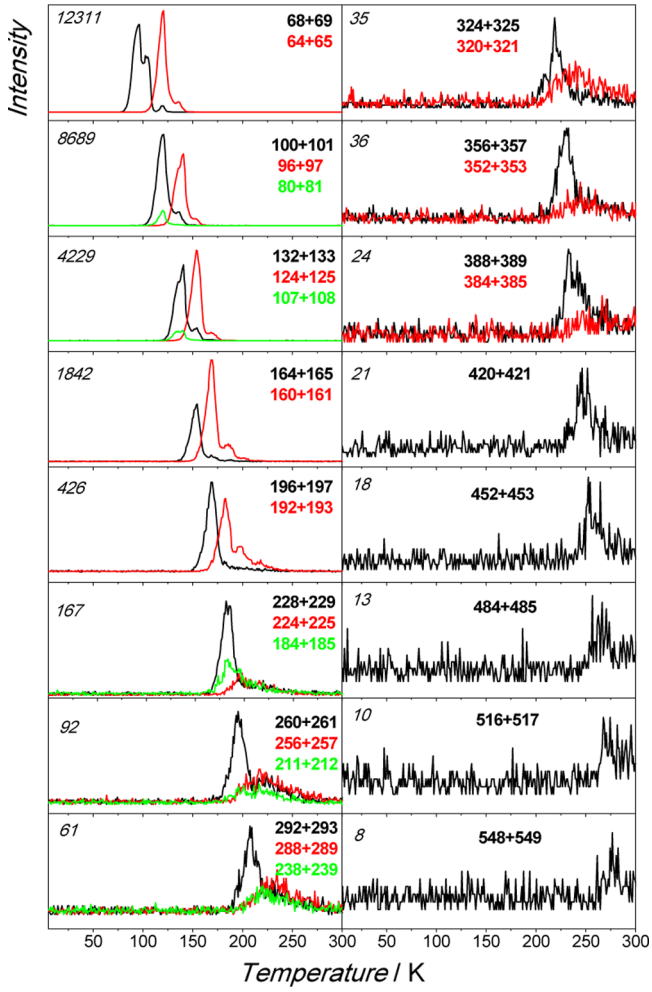

Figure 6. PI-ReTOF-MS data as a function of temperature for the indicated masses (top right in bold with formula) of the large-dose-irradiated d_4-silane sample. To obtain better a signal-to-noise ratio, two mass channels were integrated. The strongest peak intensity is shown on the left in italics. The photon energy was 10.49 eV. See the small-dose TPD curves in the Supporting Information.

Considering the TPD profiles of the ion at m/z 62, in addition to the sublimation events associated with disilane (Si_2H_6) at 95 K and to the higher-mass (^{30}Si) isotopomers of disilene (H_2SiSiH_2), i.e., the silane loss product of $Si_3H_8^+$ at 117 K, a third peak is observed at 106 K. This peak belongs to singly ionized disilane ($Si_2H_6^+$), but it is not obvious from the experimental data why the TPD peak of this species has two maxima. Possible explanations include phase changes around 100 K, different sticking of species in different layers, and trapping of disilane in heavier silanes. The slight change in the shape of the peaks and the relative intensities in the infrared spectra between 90 and 110 K (Supporting Information) do not rule out any possibility.

For n = 6 and even longer chains, the TPD maxima of $Si_nH_{2n}^+/Si_nD_{2n}^+$ depict a considerably longer tail on the high-temperature side compared to the TPD profiles of the corresponding $Si_{n+1}H_{2n+4}^+/Si_{n+1}D_{2n+4}^+$ species. This suggests that the $Si_nH_{2n}^+/Si_nD_{2n}^+$ species are formed not just by silane/d_4-silane elimination from $Si_{n+1}H_{2n+4}^+/Si_{n+1}D_{2n+4}^+$. Most likely, this can be explained by elimination of disilane (Si_2H_6) or even higher-order silanes from $Si_mH_{2m}^+/Si_mD_{2m+2}^+$ with $m > n + 1$. However, on the basis of experimental facts, the possibility that unsaturated or cyclic species also contribute to these tails cannot be completely excluded.

In contrast to the PI-ReTOF-MS spectra, due to the fragmentation, even the molecular parent peak of pentasilane ($Si_5H_{12}^+$) at m/z 152 is hardly visible in the QMS spectra recorded with electron impact ionization at 70 eV (Supporting Information). This is in agreement with the observation by Sogoshi et al.,[22] who could not directly observe species containing more than three silicon atoms via electron impact ionization in the subliming products of hydrogen atom-irradiated disilane ice. Tonokura et al. used TOF analysis coupled with VUV photoionization for the detection of pyrolysis products of disilane.[18] Although they detect species containing up to 10 silicon atoms, in their experiments the abundance of the Si_nH_{2n+2} species was ∼1 order of magnitude lower than that of the corresponding dehydrogenated Si_nH_{2n} species.

Formation Mechanism. As outlined in the Introduction, Hiraoka et al. identified disilane (Si_2H_6) in the hydrogen atom-exposed 10 K silane (SiH_4) ices.[21] The authors suggested the following mechanism for disilane (Si_2H_6) formation via successive hydrogen abstraction followed by silylene (SiH_2) insertion:

DOI: 10.1021/acs.inorgchem.6b01327
Inorg. Chem. 2016, 55, 8776−8785

Table 1. Mass-to-Charge Ratios (m/z) and Integrated Intensities (I, integration from 50 to 300 K, and from m/z−0.5 to 0.5) Observed Up to m/z 111 with the PI-ReTOF-MS Approach in Irradiated Silane (SiH_4) and d_4-Silane (SiD_4) Ices

SiH_4			SiD_4		
m/z	I	carrier	m/z	I	carrier
28	1527	$^{28}Si^{+a}$	28	1802	$^{28}Si^{+a}$
29	1672	$^{29}Si^{+,a}$ $^{28}SiH^{+a}$	29	1037	$^{29}Si^{+a}$
30	1611	$^{30}Si^{+,a}$ $^{29}SiH^{+,a}$ $^{28}SiH_2^{+a}$	30	1874	$^{30}Si^{+,a}$ $^{28}SiD^{+a}$
31	2097	$^{30}SiH^{+,a}$ $^{29}SiH_2^{+,a}$ $^{28}SiH_3^{+a}$	31	1097	$^{29}SiD^{+a}$
32	1149	$^{30}SiH_2^{+,a}$ $^{29}SiH_3^{+a}$	32	1756	$^{30}SiD^{+,a}$ $^{28}SiD_2^{+a}$
33	988	$^{30}SiH_3^{+a}$	33	923	$^{29}SiD_2^{+a}$
58	1076	$^{28}Si_2H_2^{+b}$	34	1922	$^{29}SiD_2^{+,a}$ $^{28}SiD_3^{+a}$
59	1054	$^{28}Si^{29}SiH_2^{+b}$	60	725	$^{28}Si_2D_2^{+b}$
60	89441	$^{28}Si_2H_4^{+c}$	62	1106	$^{28}Si^{29}SiD_2^{+b}$
61	27456	$^{28}Si^{29}SiH_4^{+c}$	63	2733	$^{28}Si_2D_3H^{+c,f}$
62	164618	$^{28}Si^{30}SiH_4^{+,c}$ $^{29}Si_2H_4^{+,c}$ $^{28}Si_2H_6^{+}$	64	94686	$^{28}Si_2D_4^{+c}$
63	38111	$^{29}Si^{30}SiH_4^{+,c}$ $^{28}Si^{29}SiH_6^{+}$	65	44265	$^{28}Si^{29}SiD_4^{+c}$
64	26380	$^{30}Si_2H_4^{+,c}$ $^{28}Si^{30}SiH_6^{+}$, $^{29}Si_2H_6^{+}$	66	16900	$^{28}Si^{30}SiD_4^{+,c}$ $^{29}Si_2D_4^{+c}$
65	2292	$^{29}Si^{30}Si_2H_6^{+}$	67	11097	$^{29}Si^{30}SiD_4^{+,c}$ $^{28}Si_2D_5H^{+f}$
66	1336	$^{30}Si_2H_6^{+}$	68	128849	$^{30}Si_2D_4^{+,c}$ $^{28}Si_2D_6^{+}$
72−77	10095	unresolved metastable from $Si_3H_8^{+d}$	69	37406	$^{28}Si^{29}SiD_6^{+}$
90	71872	$^{28}Si_3H_6^{+e}$	70	27429	$^{28}Si^{30}SiD_6^{+,c}$ $^{29}Si_2D_6^{+}$
91	23966	$^{28}Si_2{}^{29}SiH_6^{+e}$	71	2378	$^{29}Si^{30}SiD_6^{+}$
92	99554	$^{28}Si^{29}Si_2H_6^{+,e}$ $^{28}Si_2{}^{30}SiH_6^{+,e}$ $^{28}Si_3H_8^{+}$	72	1222	$^{30}Si_2D_6^{+}$
93	21491	$^{28}Si^{29}Si$ $^{30}SiH_6^{+,e}$ $^{29}Si_3H_6^{+,e}$ $^{28}Si_2{}^{29}SiH_8^{+}$	78−84	27763	unresolved metastable $Si_3D_8^{+d}$
94	14858	$^{29}Si_2$ $^{30}SiH_6^{+,e}$ $^{28}Si^{30}Si_2H_6^{+,e}$ $^{28}Si^{29}Si_2H_8^{+}$, $^{28}Si_2{}^{30}SiH_8^{+}$	95	2283	$^{28}Si_3D_5H^{+e,f}$
95	2388	$^{29}Si^{30}Si_2H_6^{+,e}$ $^{28}Si^{29}Si^{30}SiH_8^{+}$, $^{29}Si_3H_8^{+}$	96	67822	$^{28}Si_3D_6^{+e}$
96−103	19245	unresolved metastable from $Si_4H_{10}^{+d}$	97	22592	$^{28}Si_2{}^{29}SiD_6^{+e}$
			98	14071	$^{28}Si^{29}Si_2D_6^{+,e}$ $^{28}Si_2{}^{30}SiD_6^{+}$,
			99	6621	$^{28}Si^{29}Si^{30}SiD_6^{+,e}$ $^{29}Si_3D_6^{+,e}$ $^{28}Si_3D_7H^{+f}$
			100	96416	$^{29}Si_2{}^{30}SiD_6^{+,e}$ $^{28}Si^{30}Si_2D_6^{+,e}$ $^{28}Si_3D_8^{+}$
			101	23682	$^{29}Si^{30}Si_2D_6^{+,e}$ $^{28}Si_2{}^{29}SiD_8^{+}$
			102	17243	$^{28}Si^{29}Si_2D_8^{+}$, $^{28}Si_2{}^{30}SiD_8^{+}$
			103	2557	$^{28}Si^{29}Si^{30}SiD_8^{+}$, $^{29}Si_3D_8^{+}$
			104−111	20635	unresolved metastable $Si_4D_{10}^{+d}$

[a]From multiphoton fragmentation of $Si(H/D)_4^+$ ions or $[Si(H/D)_4]_n^+$ clusters. [b]Most likely from multiphoton fragmentation of $Si(H/D)_4^+$ ions or $[Si(H/D)_4]_n^+$ clusters. These peaks appear only below 50 K. [c]Mostly or solely $Si_2(H/D)_6^+$ by $Si(H/D)_4$ loss. [d]Due to $Si(H/D)_4$ loss in the reflectron region. [e]Mostly or solely $Si_3(H/D)_8^+$ by $Si(H/D)_4$ loss. [f]Very low-intensity peaks due to the SiD_3H impurity of SiD_4.

$$SiH_4 + H \rightarrow SiH_3 + H_2 \quad (2)$$

$$SiH_3 + H \rightarrow SiH_2 + H_2 \quad (3)$$

$$SiH_4 + SiH_2 \rightarrow Si_2H_6 \quad (4a)$$

In contrast to this, on the basis of kinetic fits of the coupled differential equations of the temporal evolution of the newly formed species, Kaiser et al. extracted the formation mechanism of disilane (Si_2H_6) in an electron-irradiated silane (SiH_4) ice by silyl radical (SiH_3) recombination:[20]

$$SiH_4 \rightarrow SiH_3 + H \quad (5)$$

$$SiH_3 + SiH_3 \rightarrow Si_2H_6 \quad (6a)$$

The two mechanisms can be distinguished by examining the products of an irradiated silane/d_4-silane (SiH_4/SiD_4) ice mixture. When all possible combinations are taken into account, eqs 4a and 6a can then be extended as follows with the mass of the isotopomers for ^{28}Si given in parentheses.

$$SiH_4 + SiD_2 \rightarrow Si_2H_4D_2\ (m/z\ 64) \quad (4b)$$

$$SiD_4 + SiH_2 \rightarrow Si_2H_2D_4\ (m/z\ 66) \quad (4c)$$

$$SiD_4 + SiD_2 \rightarrow Si_2D_6\ (m/z\ 68) \quad (4d)$$

$$SiD_3 + SiH_3 \rightarrow Si_2H_3D_3\ (m/z\ 65) \quad (6b)$$

$$SiD_3 + SiD_3 \rightarrow Si_2D_6\ (m/z\ 68) \quad (6c)$$

In the case of the mechanism of eqs 2−4, no $Si_2H_3D_3$ is expected, while for the mechanism of eqs 5 and 6a, no $Si_2H_4D_2$ and $Si_2H_2D_4$ should be present among the reaction products.

As a result of a small-dose (8 min; 15 nA; 0.5 ± 0.1 eV per molecule) irradiation of the SiH_4/SiD_4 ice, relative intensities of ion counts of 1.00 (62), 0.52 (63), 0.44 (64), 0.97 (65), 0.75 (66), 0.39 (67), and 0.72 (68) were obtained. [The relative intensities were determined by integrating the area of the peak of the $Si_2(H/D)_6$ species in the TPD curve.] Considering the ^{28}Si:^{29}Si:^{30}Si natural mass distribution of 1.000:0.051:0.034, the experimental intensity ratios mentioned above can be converted to the following relative ratios for the products: 1.00 (Si_2H_6), 0.41 (Si_2H_5D), 0.32 ($Si_2H_4D_2$), 0.88 ($Si_2H_3D_3$), 0.62 ($Si_2H_2D_4$), 0.25 (Si_2HD_5), and 0.62 (Si_2D_6). First of all, this result shows that even in the small-dose experiment, several parallel and/or consecutive processes do exist. Second, the concentration of $Si_2H_3D_3$ is roughly equal to that of the

DOI: 10.1021/acs.inorgchem.6b01327
Inorg. Chem. 2016, 55, 8776−8785

Table 2. Mass-to-Charge Ratios (m/z) and Integrated Intensities (I, integration from 50 to 300 K, and from m/z−0.5 to 0.5) Observed from m/z 112 to 600 with the PI-ReTOF-MS Approach in Irradiated Silane (SiH_4) and d_4-Silane (SiD_4) Ices[a]

SiH_4			SiD_4		
m/z	I	carrier	m/z	I	carrier
120−130	(154751)[e]	unresolved metastable from $Si_5H_{12}^+$[b]	125−137	(133923)[e]	unresolved metastable from $Si_5D_{12}^+$[b]
120	(57912)[e]	$^{28}Si_4H_8^+$[c]	124	604	$^{28}Si_4D_8^+$[c]
121	(20295)[e]	$^{29}Si^{28}Si_3H_8^+$[c]	125	(734)[e]	$^{29}Si^{28}Si_3D_8^+$[c]
122	(46806)[e]	$^{28}Si_4H_{10}^+$	128	(39971)[e]	$^{28}Si_4D_{10}^+$
123	(13215)[e]	$^{29}Si^{28}Si_3H_{10}^+$	129	(13377)[e]	$^{29}Si^{28}Si_3D_{10}^+$
145−157	(132023)[e]	unresolved metastable from $Si_6H_{14}^+$[b]	152−170	(74047)[e]	unresolved metastable from $Si_6D_{14}^+$[b]
150	(44000)[e]	$^{28}Si_5H_{10}^+$[c]	160	(19709)[e]	$^{28}Si_5D_{10}^+$[c]
151	(19010)[e]	$^{29}Si^{28}Si_4H_{10}^+$[c]	161	(7726)[e]	$^{29}Si^{28}Si_4D_{10}^+$[c]
152	(23980)[e]	$^{28}Si_5H_{12}^+$	164	(10867)[e]	$^{28}Si_5D_{12}^+$
153	(7381)[e]	$^{29}Si^{28}Si_4H_{12}^+$	165	(3159)[e]	$^{29}Si^{28}Si_4D_{12}^+$
166−176	20643	unresolved metastable from $Si_7H_{16}^+$[b]	175−190	17576	unresolved metastable from $Si_7D_{16}^+$[b]
180	14556	$^{28}Si_6H_{12}^+$[c]	192	4714	$^{28}Si_6D_{12}^+$[c]
181	11292	$^{29}Si^{28}Si_5H_{12}^+$[c]	193	2796	$^{29}Si^{28}Si_5D_{12}^+$[c]
182	13637	$^{28}Si_6H_{14}^+$	196	4845	$^{28}Si_6D_{14}^+$
183	5442	$^{29}Si^{28}Si_5H_{14}^+$	197	1967	$^{29}Si^{28}Si_5D_{14}^+$
194−205	17252	unresolved metastable from $Si_8H_{18}^+$[b]	204−216	9660	unresolved metastable from $Si_8D_{18}^+$[b]
210	6468	$^{28}Si_7H_{14}^+$[c]	224	1660	$^{28}Si_7D_{14}^+$[c]
211	6685	$^{29}Si^{28}Si_6H_{14}^+$[c]	225	1342	$^{29}Si^{28}Si_6D_{14}^+$[c]
212	7512	$^{28}Si_7H_{16}^+$	228	2410	$^{28}Si_7D_{16}^+$
213	4459	$^{29}Si^{28}Si_6H_{16}^+$	229	1258	$^{29}Si^{28}Si_6D_{16}^+$
220−235	12834	unresolved metastable from $Si_9H_{20}^+$[b]			
240−243[d]	15986	$Si_8H_{16}^+$,[c] $Si_8H_{18}^+$	256−261[d]	7086	$Si_8D_{16}^+$,[c] $Si_8D_{18}^+$
270−273[d]	10733	$Si_9H_{18}^+$,[c] $Si_9H_{20}^+$	288−293[d]	5665	$Si_9D_{18}^+$,[c] $Si_9D_{20}^+$
300−303[d]	6896	$Si_{10}H_{20}^+$,[c] $Si_{10}H_{22}^+$	320−325[d]	4091	$Si_{10}D_{20}^+$,[c] $Si_{10}D_{22}^+$
330−333[d]	4656	$Si_{11}H_{22}^+$,[c] $Si_{11}H_{24}^+$	352−357[d]	3134	$Si_{11}D_{22}^+$,[c] $Si_{11}D_{24}^+$
360−363[d]	3494	$Si_{12}H_{24}^+$,[c] $Si_{12}H_{26}^+$	384−389[d]	2640	$Si_{12}D_{24}^+$,[c] $Si_{12}D_{26}^+$
390−393[d]	2667	$Si_{13}H_{26}^+$,[c] $Si_{11}H_{28}^+$	420−421[d]	918[g]	$Si_{11}D_{28}^+$
420−423[d]	2045	$Si_{14}H_{28}^+$,[c] $Si_{14}H_{30}^+$	452−453[d]	709[g]	$Si_{14}D_{30}^+$
450−453[d]	1641	$Si_{15}H_{30}^+$,[c] $Si_{15}H_{32}^+$	484−485[d]	623[g]	$Si_{15}D_{32}^+$
480−483[d]	1332	$Si_{16}H_{32}^+$,[c] $Si_{16}H_{34}^+$	516−517[d]	553[g]	$Si_{16}D_{34}^+$
512−513[d]	641[f]	$Si_{17}H_{36}^+$	548−549[d]	492[g]	$Si_{17}D_{36}^+$
542−543[d]	566[f]	$Si_{18}H_{38}^+$			
572−573[d]	521[f]	$Si_{19}H_{40}^+$			

[a]Only the peaks of the two most abundant isotopomers are listed. The peaks of the saturated species overlap with the heavier isotopomers of the unsaturated species. [b]Due to $Si(H/D)_4$ loss in the reflectron region. [c]Mostly or solely $Si_2(H/D)_6^+$ by $Si(H/D)_4$ loss. [d]Partially resolved or unresolved peaks. The maximum of the peak is always at a m/z ratio of the $^{28}Si_n(H/D)_{2n+2}$ species. [e]The intensity is not reliable because of the overlap of peaks assigned to stable and metastable species. [f]The noise level is ∼460. [g]The noise level is ∼430.

summed concentration of $Si_2H_4D_2$ and $Si_2H_2D_4$, revealing that the silyl radical recombination and the silylene insertion are equally important parallel processes. Finally, the appearance of the Si_2H_5D and Si_2HD_5 products indicates that additional processes such as H ↔ D exchange reactions take place (reaction 7). These exchanges might be initiated by suprathermal hydrogen atoms holding kinetic energies of a few electron volts (a few hundred kilojoules per mole), thus overcoming barriers to hydrogen/deuterium abstraction from closed shell species easily.[44]

$$SiH_4 + D \rightarrow SiH_3D + H \quad (7a)$$

$$SiD_4 + H \rightarrow SiHD_3 + D \quad (7b)$$

Considering the formation of higher-order silanes, the most likely main formation routes are the reactions analogous to eqs 5 and 6, i.e., reactions 8 and 9, a stepwise buildup of silanes via reactions of two silyl-type radicals

$$H{-}Si_nH_{2n}{-}SiH_3 \rightarrow H{-}Si_nH_{2n}{-}SiH_2 + H \quad (8)$$

$$H{-}Si_nH_{2n}{-}SiH_2 + SiH_3 \rightarrow H{-}Si_nH_{2n}{-}SiH_2{-}SiH_3 \quad (9)$$

and silylene insertions

$$H{-}Si_nH_{2n}{-}SiH_3 + SiH_2 \rightarrow H{-}Si_nH_{2n}{-}SiH_2{-}SiH_3 \quad (10)$$

CONCLUSIONS

In this study, we have provided compelling evidence that exposure of silane (SiH_4) and d_4-silane (SiD_4) ices to energetic electrons produced higher-order silanes up to nonadecasilane ($Si_{19}H_{40}$). It is also revealed that the vacuum ultraviolet (VUV) single-photon ionization PI-ReTOF-MS technique represents an extremely powerful method for detecting the irradiation products upon sublimation because unlike in EI-QMS, parent ions ($Si_nH_{2n+2}^+$) can be easily observed in the PI-ReTOF-MS spectra. Further, the $Si_{n-1}H_{2n-2}^+$ ions mostly, or solely, appear in the PI-ReTOF-MS spectra as a consequence of loss of SiH_4 from the saturated parent ions ($Si_nH_{2n+2}^+$), not because of the ionization of unsaturated $Si_{n-1}H_{2n-2}$ silenes. Because the

DOI: 10.1021/acs.inorgchem.6b01327
Inorg. Chem. 2016, 55, 8776−8785

presence of Si_2H_4 isomers in the low-temperature irradiated ices was determined via infrared spectroscopy, we can conclude that the silenes do not survive the sublimation. Most likely, they might react either with hydrogen atoms that are produced by the irradiation process and mobilized upon heating or with each other. The former process results in saturated silanes; the latter can produce larger polymers, including high-mass saturated silanes. In contrast to this, this study revealed that silanes can, at least partially, survive the sublimation into high vacuum. In the investigated temperature range (5.5−300 K), even $Si_{19}H_{40}^+$ could be observed at ∼300 K. This species contains four more silicon atoms than the largest silane observed so far. From the TPD profiles, the sublimation temperature of the silane (Si_nH_{2n+2}) species could be deduced, and these data are summarized in Figure 7. According to this, the fractional

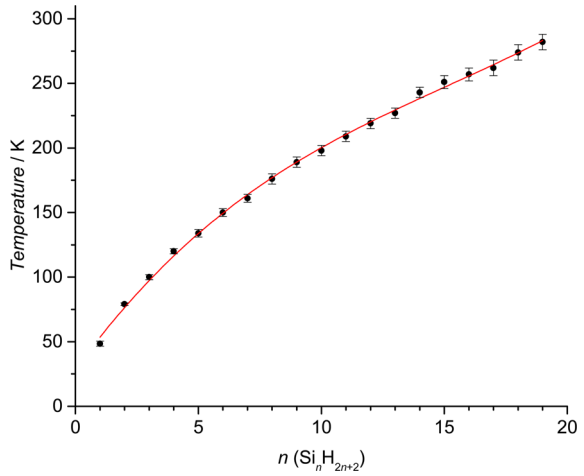

Figure 7. Sublimation temperature as determined via onset values of the TPD curves of the silanes (Si_nH_{2n+2}). The sublimation temperatures of the corresponding Si_nD_{2n+2} species agree with those of their nondeuterated analogues better than the estimated error bar.

sublimation is a suitable method for partial separation of higher-order silanes. Finally, it is found that silane (SiH_4) is more reactive than d_4-silane (SiD_4); considering that the unimolecular decomposition of silane/d_4-silane produced atomic hydrogen/deuterium, energy and momentum conservation dictated that if the transferred energy from the electron to the Si−H/Si−D bond is equivalent, less energy is available for the kinetic energy of the deuterium compared to the hydrogen atom. Therefore, as also elucidated for the methane versus d_4-methane system,[45] the likelihood of a hydrogen atom escaping from the matrix cage forming the reactive silyl radical is higher than the likelihood of a deuterium atom escaping the cage, leading to the synthesis of the d_3-silyl radical. It should also be noted that the larger tunneling rate of hydrogen atoms compared to that of deuterium atoms such as in eqs 2 and 3 might also contribute to some extent to the higher reactivity of silane. The possible role of tunneling in these reactions was discussed by Hiraoka et al.[21] Therefore, upon exposure to energetic electrons, silane produces more reactive species than d_4-silane does, which in turn leads to a greater variety and more complex silanes.

■ ASSOCIATED CONTENT

Supporting Information

The Supporting Information is available free of charge on the ACS Publications website at DOI: 10.1021/acs.inorgchem.6b01327.

UV−vis spectrum of the deposited and the irradiated d_4-silane ice, refractive indices of SiH_4 and SiD_4 as a function of wavelength, pressure TPD curves, change in the low-wavenumber part of the IR spectrum upon heating the large-dose-irradiated SiH_4 ice from 80 to 120 K, PI-ReTOF-MS data as a function of temperature of small-dose-irradiated silane and d_4-silane samples, and comparison of EI-QMS and PI-ReTOF-MS spectra (PDF)

■ AUTHOR INFORMATION

Corresponding Authors

*E-mail: tarczay@chem.elte.hu.

*E-mail: ralfk@hawaii.edu.

Present Addresses

†G.T. is a Visiting Fulbright Professor. Permanent address: Laboratory of Molecular Spectroscopy, Institute of Chemistry, Eötvös University, P.O. Box 32, H-1518 Budapest 112, Hungary.

‡M.F.: Berlin Institute of Technology, IOAP, Hardenbergstrasse 36, 0623 Berlin, Germany.

Notes

The authors declare no competing financial interest.

■ ACKNOWLEDGMENTS

The authors thank the National Science Foundation (NSF) for support under Grant CHE-1360658. G.T. thanks the Fulbright Foundation and the Hungarian Scientific Research Fund for financial support (OTKA K108649). M.F. acknowledges funding from the Deutsche Forschungsgemeinschaft DFG (FO 941/1). G.T. acknowledges helpful discussion with Dr. Roland Szalay (Eötvös University, Budapest, Hungary).

■ REFERENCES

(1) Filtvedt, W. O.; Holt, A.; Ramachandran, P. A.; Melaaen, M. C. *Sol. Energy Mater. Sol. Cells* **2012**, *107*, 188−200.

(2) Furusawa, M.; Tanaka, H. Liquid Silicon Materials. In *Solution Processing of Inorganic Materials*; Mitzi, D. B., Ed.; Wiley: Hoboken, NJ, 2009; pp 131−155.

(3) Reedijk, J., Poeppelmeier, K. R., Eds. *Comprehensive Inorganic Chemistry II*, 2nd ed.; Elsevier: Amsterdam, 2013.

(4) Shimoda, T.; Matsuki, Y.; Furusawa, M.; Aoki, T.; Yudasaka, I.; Tanaka, H.; Iwasawa, H.; Wang, D.; Miyasaka, M.; Takeuchi, Y. *Nature* **2006**, *440*, 783−786.

(5) Hidding, B.; Pfitzner, M.; Simone, D.; Bruno, C. *Acta Astronaut.* **2008**, *63*, 379−388.

(6) Goldhaber, D. M.; Betz, A. L. *Astrophys. J.* **1984**, *279*, L55−L58.

(7) Kaiser, R. I.; Osamura, Y. *Astron. Astrophys.* **2005**, *432*, 559−566.

(8) Bains, W. *Astrobiology* **2004**, *4*, 137−167.

(9) Feigl, A.; Bockholt, A.; Weis, J.; Rieger, B. Modern synthetic and Application Aspects of Polysilanes: An Underestimated Class of Materials? In *Silicon Polymers*; Muzafarov, A. M., Ed.; Springer: Dordrecht, The Netherlands, 2011.

(10) Rivard, E. *Chem. Soc. Rev.* **2016**, *45*, 989−1003.

(11) Fehér, F.; Schinkitz, D.; Schaaf, J. *Z. Anorg. Allg. Chem.* **1971**, *383*, 303−313.

(12) Fehér, F.; Schinkitz, D.; Wronka, G. *Z. Anorg. Allg. Chem.* **1971**, *384*, 226−230.

DOI: 10.1021/acs.inorgchem.6b01327
Inorg. Chem. 2016, 55, 8776−8785

(13) Fehér, F.; Schinkitz, D.; Strack, H. *Z. Anorg. Allg. Chem.* **1971**, *385*, 202−208.
(14) Fehér, F.; Baier, H.; Enders, B.; Krancher, M.; Laakmann, J.; Ocklenburg, F. J.; Skrodski, D. *Z. Anorg. Allg. Chem.* **1985**, *530*, 191−195.
(15) Kvaratskheli, Y. K.; Zhirkov, M. S.; Lobachev, Y. A.; Fadeev, L. L. *Khim. Tekhnol.* **2005**, *3*, 2−6.
(16) Miyagawa, H.; Itoh, M.; Abe, T.; Iwata, K.; Koizumi, K. Silicon Hydrides. EP149363A2, 1985.
(17) Brausch, N.; Ebbers, A.; Stochniol, G.; Trocha, M.; Oenal, Y.; Sauer, J.; Stuetzel, B.; Wolf, D.; Stueger, H. Process for Preparing Higher Hydridosilanes. WO2010003729A1, 2010.
(18) Tonokura, K.; Murasaki, T.; Koshi, M. *J. Phys. Chem. B* **2002**, *106*, 555−563.
(19) Auner, G. A.; Bauch, C.; Lippold, G.; Deltschew, R. Processing and Use of Halogenated Polysilanes. WO2008009473A1, 2008.
(20) Sillars, D.; Bennett, C. J.; Osamura, Y.; Kaiser, R. I. *Chem. Phys. Lett.* **2004**, *392*, 541−548.
(21) Hiraoka, K.; Sato, T.; Sato, S.; Hishiki, S.; Suzuki, K.; Takahashi, Y.; Yokoyama, T.; Kitagawa, S. *J. Phys. Chem. B* **2001**, *105*, 6950−6955.
(22) Sogoshi, N.; Sato, S.; Takashima, H.; Sato, T.; Hiraoka, K. *Chem. Lett.* **2009**, *38*, 986−987.
(23) Turner, A. M.; Abplanalp, M. J.; Chen, S. Y.; Chen, Y. T.; Chang, A. H. H.; Kaiser, R. I. *Phys. Chem. Chem. Phys.* **2015**, *17*, 27281−27291.
(24) Abplanalp, M. J.; Borsuk, A.; Jones, B. M.; Kaiser, R. I. *Astrophys. J.* **2015**, *814*, 45.
(25) Jones, B. M.; Kaiser, R. I. *J. Phys. Chem. Lett.* **2013**, *4*, 1965−1971.
(26) Abplanalp, M. J.; Förstel, M.; Kaiser, R. I. *Chem. Phys. Lett.* **2016**, *644*, 79−98.
(27) Heavens, O. S. *Optical Properties of Thin Solid Films*; Scientific Publications Butterworths: London, 1965.
(28) Groner, P.; Stolkin, I.; Gunthard, H. H. *J. Phys. E: Sci. Instrum.* **1973**, *6*, 122−123.
(29) Drouin, D.; Couture, A. R.; Joly, D.; Tastet, X.; Aimez, V.; Gauvin, R. *Scanning* **2007**, *29*, 92−101.
(30) Sears, W. M.; Morrison, J. A. *J. Chem. Phys.* **1975**, *62*, 2736−2739.
(31) Maity, S.; Kaiser, R. I.; Jones, B. M. *Faraday Discuss.* **2014**, *168*, 485−516.
(32) VonDrasek, W. A.; Okajima, S.; Hessler, J. P. *Appl. Opt.* **1988**, *27*, 4057−4061.
(33) Andrews, L.; Wang, X. *J. Phys. Chem. A* **2002**, *106*, 7696−7702.
(34) Sernelius, B. E. *Surface modes in physics*; John Wiley & Sons: New York, 2011.
(35) Weaver, J.; Olson, C.; Lynch, D. W. *Phys. Rev. B* **1977**, *15*, 4115−4118.
(36) Lightfoot, P. D.; Becerra, R.; Jemi-Alade, A. A.; Lesclaux, R. *Chem. Phys. Lett.* **1991**, *180*, 441−445.
(37) Albinsson, B.; Teramae, H.; Plitt, H. S.; Goss, L. M.; Schmidbaur, H.; Michl, J. *J. Phys. Chem.* **1996**, *100*, 8681−8691.
(38) Itoh, U.; Toyoshima, Y.; Onuki, H.; Washida, N.; Ibuki, T. *J. Chem. Phys.* **1986**, *85*, 4867−4872.
(39) Maier, G.; Reisenauer, H. P.; Glatthaar, J. *Chem. - Eur. J.* **2002**, *8*, 4383−4391.
(40) Ruscic, B.; Berkowitz, J. *J. Chem. Phys.* **1991**, *95*, 2407−2415.
(41) Berkowitz, J.; Greene, J. P.; Cho, H.; Ruscic, B. *J. Chem. Phys.* **1987**, *86*, 1235−1248.
(42) George, M. A. R.; Savoca, M.; Dopfer, O. *Chem. - Eur. J.* **2013**, *19*, 15315−15328.
(43) Bock, H.; Ensslin, W.; Feher, F.; Freund, R. *J. Am. Chem. Soc.* **1976**, *98*, 668−674.
(44) (a) Kaiser, R. I.; Eich, G.; Gabrysch, A.; Roessler, K. *Astrophys. J.* **1997**, *484*, 487−498. (b) Bennett, C. J.; Jamieson, C. S.; Osamura, Y.; Kaiser, R. I. *Astrophys. J.* **2005**, *624*, 1097−1105. (c) Kaiser, R. I.; Roessler, K. *Astrophys. J.* **1997**, *475*, 144−154. (d) Bennett, C. J.; Kaiser, R. I. *Astrophys. J.* **2007**, *660*, 1289−1295. (e) Zheng, W.; Jewitt, D.; Kaiser, R. I. *Astrophys. J.* **2006**, *648*, 753−761.
(45) Kaiser, R. I.; Roessler, K. *Astrophys. J.* **1998**, *503*, 959−975.

DOI: 10.1021/acs.inorgchem.6b01327
Inorg. Chem. 2016, 55, 8776−8785